Regular Article - Theoretical Physics

Analysis of the $\psi(3770)$ resonance in line with unitarity and analyticity constraints

Christoph Hanhart[1] , **Stephan Kürten**[2,3], **Méril Reboud**[4,a] , **Danny van Dyk**[5]

[1] Institute for Advanced Simulation and Institut für Kernphysik, Forschungszentrum Jülich, 52425 Jülich, Germany
[2] Physik Department T31, Technische Universität München, 85748 Garching, Germany
[3] Helmholtz-Institut für Strahlen- und Kernphysik (Theorie), Bethe Center for Theoretical Physics, Universität Bonn, 53115 Bonn, Germany
[4] Theoretische Physik 1, Naturwissenschaftlich-Technische Fakultät, Universität Siegen, 57068 Siegen, Germany
[5] Institute for Particle Physics Phenomenology and Department of Physics, Durham University, Durham DH1 3LE,, UK

Abstract We study the inclusive and exclusive cross sections of $e^+e^- \to$ hadrons for center-of-mass energies between 3.70 and 3.83 GeV to infer the mass, width, and couplings of the $\psi(3770)$ resonance. By using a coupled-channel K-matrix approach, we setup our analysis to respect unitarity and the analyticity properties of the underlying scattering amplitudes. We fit several models to the full dataset and identify our nominal results through a statistical model comparison. We find that, accounting for the interplay between the $\psi(2S)$ and the $\psi(3770)$, no further pole is required to describe the $\psi(3770)$ line shape. In particular we derive from the pole location $M_{\psi(3770)} = 3778.8 \pm 0.3$ MeV and $\Gamma_{\psi(3770)} = 25.0 \pm 0.5$ MeV. Moreover, we find the decay to D^+D^- and $D^0\bar{D}^0$ to be consistent with isospin symmetry and derive an upper bound on the branching ratio $\mathcal{B}(\psi(3770) \to \text{non-}D\bar{D}) < 6\%$ at 90% probability.

1 Introduction

The study of $e^+e^- \to$ hadrons processes has been useful to improve our understanding of a variety of aspects of particle physics in general and the strong interaction in particular. These include the confirmation of three as the number of strong charges (colours) [1], the discovery of exotic states outside the established quark model (see Refs. [2–7] for recent reviews), and the data-driven prediction of hadronic contributions to the anomalous magnetic moment of the muon [8].

In this analysis, we study $e^+e^- \to$ open charm processes in the immediate vicinity of the $D^0\bar{D}^0$ and the D^+D^- thresholds but below the $D\bar{D}^* +$ h.c. threshold. Our study

of $e^+e^- \to$ open charm data is motivated by the following questions:

1. What is the nature of the $\psi(3770)$ state? To that end, does it decay sizeably into non-$D\bar{D}$ final states, in contradiction with being a pure $c\bar{c}$ quarkonium state and in support of alternative interpretations?
2. Are contemporary theoretical frameworks capable to describe the now-available high-resolution measurements of $e^+e^- \to$ open charm processes?
3. How many vector states are necessary to descibe the data within the mass range studied?
4. Can we describe the $e^+e^- \to$ open charm spectrum well enough to use it for data-driven predictions of non-local contributions in $b \to s\ell^+\ell^-$ processes?

A previous study covering a large part of the $e^+e^- \to$ open charm phase space has been carried out in Ref. [9]; it uses, amongst others, high resolution BES, BESII, and BESIII data. That study uses a model consisting of a sum of Breit–Wigner functions. This approach is known to violate unitarity of the S-matrix in the description of broad resonances close to their dominant decay threshold (see Review *Resonances* in Ref. [10]), which clearly holds for the $\psi(3770)$. As a consequence, the line shape extracted from $e^+e^- \to$ open charm data cannot be transferred to other applications, such as data-driven predictions of $b \to s\ell^+\ell^-$ decays, without incurring an unquantifiable model uncertainty. To overcome this issue, we strive to model the relevant scattering amplitudes with as few assumptions as possible before fitting our models to the available data. Our choice of phase space window implies the absence of dominant three-hadron final states. This is a necessary prerequisite for the

a e-mail: merilreboud@gmail.com (corresponding author)

K-matrix framework, which we use in this study. A previous K-matrix analysis of exclusive $e^+e^- \to$ open charm data has been carried out in Ref. [11], exclusively using Belle data. This data covers a much larger energy range than what we study here but features a substantially lower resolution than the BES data. It is therefore interesting to see if the available high-resolution measurements by the BES, BESII, and BESIII experiments can be described within the highly-predictive K-matrix framework. Moreover, we allow for the $\psi(2S)$ to interfere with the $\psi(3770)$, which appears necessary to describe the data.

Conceptually our work seems similar to that of Ref. [12], however, we deviate in a couple of crucial points: we allow for non-$D\bar{D}$ decays and for a contribution of the $\psi(2S)$. The most salient difference is that our framework does not generate additional poles beyond those explicitly included by construction. A more detailed comparison to the results of Ref. [12] will be presented below.

The structure of this article is as follows. We discuss our analysis setup in Sect. 2, including a brief overview of the K-matrix framework, a description of the available experimental data, and the definition of our fit models. We present the numerical results in Sect. 3. A summary and outlook follows in Sect. 4. We describe a path toward data-driven predictions of the non-local form factors in rare semileptonic b decays in App. A.

2 Setup

2.1 Analysis framework

The K-matrix framework has first been proposed in Ref. [13] to describe $2 \to r \to 2$ scattering amplitudes and $r \to 2$ decay amplitudes, where r denotes some hadronic resonance. The framework allows straightforwardly for the inclusion of two-body channels and automatically leads to unitary amplitudes. Here, we apply the K-matrix framework in its modern, Lorentz-invariant form; see Ref. [10] for a review and a collection of the relevant formulae.

In the K-matrix framework, a scattering amplitude $\mathcal{M}$ is modelled as

$$\mathcal{M} = n \, [1 - \mathcal{K} \, \Sigma]^{-1} \, \mathcal{K} \, n. \tag{1}$$

Here, columns and rows of $\mathcal{M}$ correspond to the initial and final states of the processes under consideration, which are commonly referred to as "channels". The same holds for the columns and rows of the underlying matrix $\mathcal{K}$. Moreover, to ensure unitarity of the S-matrix and to uphold symmetry under time-reversal, $\mathcal{K}$ must be real-valued and symmetric, respectively. The channels' vertex structure is accounted for by the diagonal matrix $n = \mathrm{diag}(n_a, n_b, ...)$ with

$$n_k = (q_k/q_0)^{l_k} \, F_{l_k}(q_k/q_0). \tag{2}$$

In the above, l_k is the orbital angular momentum in channel k and

$$q_k(s) = \frac{\lambda(s, M_{k1}^2, M_{k2}^2)^{1/2}}{2\sqrt{s}} \tag{3}$$

is the break-up momentum, expressed in terms of the Källén triangle function. The masses of the two hadrons of channel k are denoted by M_{k1} and M_{k2}, respectively. Their break-up momentum is further used to define a channel's phase space function $\rho_k = q_k(s)/(8\pi\sqrt{s})$. Moreover, q_0 is some fixed momentum scale, conventionally chosen between $0.2\,\mathrm{GeV}$ and $1\,\mathrm{GeV}$ [10,14], and F_{l_k} are the Blatt-Weisskopf form factors [15]

$$F_0^2(z) = 1, \qquad F_1^2(z) = 1/(1 + z^2).$$

The matrix Σ in Eq. (1) is a diagonal matrix $\Sigma = \mathrm{diag}(\Sigma_a(s), \Sigma_b(s), ...)$, where the functions $\Sigma_k(s)$ are channel-specific, modified Chew–Mandelstam functions. The latter functions are the proper analytic completions of the phase space factors $i\rho_k(s)n_k(s)^2$ by means of dispersion integrals, which allow for the continuations of the amplitudes into the complex plane. Here, we are only concerned with channels for which $M_{k1} = M_{k2}$, which is reflected in the formulas for the modified Chew–Mandelstam functions. For an S-wave channel (i.e., $l_k = 0$), they read

$$\Sigma_k(s) = \frac{1}{8\pi^2} \Pi_0. \tag{4}$$

For a P-wave channel (i.e., $l_k = 1$) they read

$$\Sigma_k(s) = \frac{1}{8\pi^2} \frac{s - s_{\mathrm{th}}}{s_0} \left(F_1^2(q_k(s)/q_0) \, \Pi_0(s) + \Pi_1(s) \right). \tag{5}$$

In the above we use

$$\Pi_0 = -\frac{\sqrt{s_{\mathrm{th}} - s}}{\sqrt{s}} \arctan\sqrt{\frac{s}{s_{\mathrm{th}} - s}}, \tag{6}$$

$$\Pi_1 = \frac{s_0^{3/2}}{\sqrt{s_0 - s_{\mathrm{th}}}(s + s_0 - s_{\mathrm{th}})} \mathrm{atanh}\sqrt{1 - \frac{s_{\mathrm{th}}}{s_0}}, \tag{7}$$

where $s_{\mathrm{th}} = 4M_k^2$ and $s_0 = 4q_0^2$. Note that the pole in Eq. (7) cancels exactly the pole due to F_1^2, which makes both Σ_k analytic functions of s in the whole complex plane, except for a branch cut starting at $s = s_{\mathrm{th}}$. This branch cut connects the two Riemann sheets of the Chew–Mandelstam functions. The formulas above are suitable to evaluate them on their first Riemann sheet only. To evaluate the function on their second Riemann sheet, we use

$$\Sigma_k^{\mathrm{II}}(s) = \Sigma_k(s) + 2i \left(\rho_k(s^*) \, n_k^2(s^*) \right)^*. \tag{8}$$

Following Ref. [10], we parametrize the K-matrix as follows:

$$\mathcal{K}_{ij}(s) = \sum_{r=1}^{N_R} \frac{g_i^r g_j^r}{m_r^2 - s} + c_{ij} \,. \tag{9}$$

The first term describes the N_R resonances included explicitly in the model, with bare mass m_r and g_i^r for their coupling to the channel i, all of them real valued. The second term is the background constant that models non-resonant contributions of, e.g., tails of resonances outside the phase space window considered here.

Each resonance r gives rise to pairs of poles of the scattering amplitudes Eq. (1) on the unphysical Riemann sheets. For N_C channels, this amounts to a total of 2^{N_C} Riemann sheets. However, given the parametrisation employed here, it is sufficient to continue the individual self-energies Σ_k to their second sheet to reach those poles. We may label any given sheet with a multi index, by denoting on which sheet the respective self-energy for each channel is evaluated. In this notation, the physical sheet is denoted as $\mathrm{I} \equiv \{\mathrm{I}, \ldots, \mathrm{I}\}$. The resonance pole located closest to the physical axis is commonly quoted as the resonance pole and parametrised as

$$\sqrt{s_r} = M_r - i \frac{\Gamma_r}{2}, \tag{10}$$

which defines the resonance's physical mass M_r and total decay width Γ_r. To access these properties, one requires the numerical evaluation of the scattering amplitudes on the proper Riemann sheet. In our analysis, we are interested only in the description of the $\psi(3770)$ pole, which is located above all modelled hadronic thresholds. To determine this pole's properties, it therefore suffices to consider the Riemann sheet closest to the physical axis, which we denote as $\mathrm{II} \equiv \{\mathrm{II}, \ldots, \mathrm{II}\}$.

This sheet can be reached by means of

$$\mathcal{M}^{\mathrm{II}} = n \left[1 - \mathcal{K} \, \Sigma^{\mathrm{II}} \right]^{-1} \mathcal{K} \, n \,, \tag{11}$$

where Σ^{II} denotes the self-energy matrix with all channel-self-energies continued to their second sheet. To determine the physical quantities, such as partial decay widths and branching ratios, we require access to the renormalized couplings G_k^r. We extract these couplings as residues of the diagonal elements in channel space of a partial-wave amplitude on the proper Riemann sheet

$$(G_k^r)^2 = -\frac{1}{2\pi i} \oint_{C(s_r)} ds \, \mathcal{M}_{kk}^{\mathrm{II}}(s). \tag{12}$$

Here $C(s_r)$ describes a contour around the resonance's pole position, s_r, on the proper Riemann sheet that avoids all other singularities. The definition of the physical observables then reads

$$\Gamma_{r \to a} = \frac{|G_a^r|^2}{M_r} \rho_a(M_r^2) \quad \text{and} \quad \mathcal{B}_{r \to a} = \frac{\Gamma_{r \to a}}{\Gamma_r} \tag{13}$$

where we employed the narrow width approximation for the calculation of the partial width. Note that we do not impose the identity $\Gamma_r = \sum_a \Gamma_{r \to a}$. We discuss this type of relation later on in Sect. 2.3. Finally, we compute the cross sections from the scattering amplitudes as

$$\sigma_{e^+ e^- \to k}(s) = \frac{1}{16\pi s} \frac{\rho_k(s)}{\rho_{e^+ e^-}(s)} \frac{\mathcal{N}_k}{4} \left| \mathcal{M}_{e^+ e^-, k} \right|^2, \tag{14}$$

where $\mathcal{N}_k = 2l_k + 1$ is a combinatorial factor and the factor of 4 accounts for the number of spin configurations in the initial state.

Resonances For this analysis, we study cross sections for exclusive $e^+ e^- \to$ open charm processes. All resonances must share the same quantum numbers as the photon, i.e., all flavour quantum numbers must vanish and $J^{PC} = 1^{--}$, where J denotes the total angular momentum. The energy range of interest here, $4M_{D^0}^2 < s < (M_D + M_{D^*})^2$, sits above the well-known narrow charmonium resonances J/ψ and $\psi(2S)$ and is dominated by effects of the broad $\psi(3770)$ resonance. We do not aim at modelling the shape of the J/ψ and $\psi(2S)$ resonances. Nevertheless, the interference effect between the $\psi(2S)$ and the $\psi(3770)$ is found to play a major role in the shape of the $\psi(3770)$ in various works [9,11]. Hence, we include the $\psi(2S)$ as the closest narrow charmonium state in our model:

$$r \in \{\psi(2S), \psi(3770)\} \quad \text{and} \quad N_R = 2 \,. \tag{15}$$

Channels The energy range of interest overlaps with only a small slice of the full phase space of open-charm production. The dominant processes are therefore $e^+ e^- \to$ non-$D\bar{D}$, $e^+ e^- \to D^+ D^-$, and $e^+ e^- \to D^0 \bar{D}^0$. A comment is due on the hadronic non-$D\bar{D}$ final states. Empirically, it is known that various genuine non-two-body final states contribute here [10] that cannot be straightforwardly expressed within the K-matrix framework as applied here [10,13]. For our purpose, this inclusive final state is expected to yield a numerically dominant contribution only to the decay width of the $\psi(2S)$ resonance, i.e., well below the open charm threshold. We therefore setup our model using the following assumptions:

- The effects of the $\psi(2S)$ modify the line shape of the $\psi(3770)$ and a description of this modification is needed. However, we are not interested in describing the line shape of the $\psi(2S)$. For the purpose of determining the impact on the $\psi(3770)$ line shape through interference, we model this component as an effective P-wave two-body channel eff$_{\psi(2S)}$ with threshold $4M_\pi^2$. Note that the

results are insensitive to the concrete value chosen here as long as it is located significantly below the energy range considered.

Moreover, we allow for a non-vanishing non-$D\bar{D}$ component to the decay width of the $\psi(3770)$. For the purpose of determining the overall width of the $\psi(3770)$ we model this component as an effective P-wave two-body channel $\text{eff}_{\psi(3770)}$ with threshold $4M_\pi^2$. We study two scenarios: one in which $\text{eff}_{\psi(3770)}$ and $\text{eff}_{\psi(2S)}$ are assumed to be distinct and hence non-interfering; and one in which the channels are identical, $\text{eff}_{\psi(3770)} = \text{eff}_{\psi(2S)} = \text{eff}_\psi$.

- The cross sections in our phase space windows are dominated by D^+D^- and $D^0\bar{D}^0$ final states. We model these final states via two independent P-wave channels (i.e., $l_{D^+D^-} = l_{D^0\bar{D}^0} = 1$).
- The coupling of the two resonances to e^+e^- enter all cross sections discussed here. To keep our numerical code as simple as possible, we define a K-matrix channel with label e^+e^-. This approach leads to an inadvertent accounting for hadronic open-charm contributions to the e^+e^- vacuum polarisation, which is negligible in our case. We have checked that our numerical code yields virtually indistinguishable results compared to a (simpler) code that uses a P-vector approach for the e^+e^- channel. We model the e^+e^- initial state as an S-wave channel (i.e., $l_{e^+e^-} = 0$).

This leaves us with the following sets of channels, depending on the number of non-$D\bar{D}$ channels included. Each channel features an independent set of couplings. We thus have either $N_C = 5$ with

$$k \in \{e^+e^-, D^+D^-, D^0\bar{D}^0, \text{eff}_{\psi(2S)}, \text{eff}_{\psi(3770)}\}, \qquad (16)$$

or $N_C = 4$ with

$$k \in \{e^+e^-, D^+D^-, D^0\bar{D}^0, \text{eff}_\psi\}. \qquad (17)$$

2.2 Experimental data

Experimental measurements of the $e^+e^- \rightarrow$ hadron cross sections in the energy range of interest are available from the BaBar [16], Belle [17], BES [18], BESII [19], BESIII [20], and CLEO [21] experiments. These measurements vary strongly in the underlying approaches to measure the cross sections, which can roughly be divided into two categories:

energy scan The BES, BESII, BESIII, and CLEO experiments take data at a variety of different center-of-mass energies, $\sqrt{s}$, of the e^+e^- collisions. This enables them to obtain measurements of the exclusive cross sections at different values of $\sqrt{s}$. The resolution of these data points is $\lesssim 10$ MeV, yielding high-resolution measurements

of the spectra. In the context of this analysis, we treat energy-scan measurements as single-points with vanishing bin width.

initial-state radiation The BaBar and Belle experiments work at fixed center-of-mass energies, $\sqrt{s} \sim 10$ GeV, far above the energy range of interest. Nevertheless, they can access lower energies by means of initial-state radiation (ISR), i.e., radiation of an energetic photon off either of the initial-state leptons. This approach does not permit a high-resolution energy scan of the pertinent cross section. Instead, those results are presented as integrated cross sections in relatively coarse bins of the center-of-mass energy.

For this analysis, we use only the measurements by the BES, BESII, and BESIII experiments. Our reasoning is as follows:

- The BES, BESII, and BESIII measurements are based on much larger data sets than the CLEO measurements. Consequently, the latter are not competitive with the former within our analysis on account of larger statistical uncertainties.
- The BES, BESII, and BESIII measurements provide a high-resolution access to the energy dependence of the exclusive cross sections. The BaBar and Belle results cannot compete with these BES results due the limitations of the ISR method.

We refer to the data sets on the ratio $R = \sigma(e^+e^- \rightarrow \text{hadrons})/\sigma(e^+e^- \rightarrow \mu^+\mu^-)$ as inclusive data and to the data sets on $e^+e^- \rightarrow D^0\bar{D}^0$ and $e^+e^- \rightarrow D^+D^-$ as the exclusive data. Taking the exclusive data into account allows our fit to be sensitive to isospin symmetry violation. We only use data points with center-of-mass energy $\sqrt{s} \leq 3.83$ GeV, to limit the experimental pollution of the $\psi(4040)$ resonance. This leaves us with the following combined dataset that is used throughout our analyses:

inclusive We use 12 and $60 + 1$ experimental measurements from the analyses by BES [18] and BESII [19,22], denoted as `BES 2002`, `BESII 2006A` and `BESII 2006B`, respectively, in the rest of this paper;
exclusive We use 26 and 27 experimental measurements from a preliminary BESIII analysis [23] that we will denote as `BESIII 2017` in the following. We do not account for small systematic correlations between the D^+D^- and $D^0\bar{D}^0$ final states. The observed cross section σ^{obs} still needs to be converted to the Born cross section σ^{B}. This is achieved by [24]

$$\sigma^{\text{B}}(E) = \sigma^{\text{obs}}(E) \frac{|1 - \Pi(E)|^2}{1 + \delta(E)},$$

where $\Pi(E)$ is the vacuum polarization and $\delta(E)$ is the radiative correction that accounts for initial-state radiation. This is done to ensure consistency of our analysis with respect to the inclusive cross section measurements.

This corresponds to a total of 126 observations. As they are measured during different experimental runs, all these measurements are statistically independent. The systematic uncertainties are provided in the experimental publication. They permit us to reconstruct the full correlation matrices by separating the energy-independent uncertainties from the other systematic uncertainties.

We fix the value of the R ratio below the open-charm threshold to the value $R_{uds} = 2.171$ [25]. To ensure the convergence of the fits and the physical meaning of the models, we furthermore consider two additional constraints:

– The bare partial width of the $\psi(2S)$ resonance to e^+e^- is constrained to $\Gamma_{\psi(2S)\to e^+e^-} = (2.33 \pm 0.04)$ keV. This constraint has a limited impact on the fit and is just used to ensure convergence.
– The value of the R ratio far above the open-charm threshold should not exceed the value $R_{udsc} = 3.55$ [25]. To implement this constraint, in the fit we impose a penalty function

$$-2\log P \supseteq \frac{(r-3.55)^2}{\sigma^2}\theta(r-3.55), \qquad (18)$$

where $r = R(\sqrt{s} = 9\,\text{GeV})$ corresponds to the four-flavour R ratio evaluated below the first $b\bar{b}$ resonance and θ is the Heaviside function. We use $\sigma = 10\%$ to account for the theory uncertainty of the R ratio prediction. Here again, the fit is not sensitive to these exact values, but using this prior ensures that the model remains physical.

2.3 Analysis

To confront our physical model with the available data, we perform a Bayesian analysis. Central to this type of analysis is the posterior probability density function (PDF) of our fit parameters ϑ,

$$P(\vartheta \mid D, M) = \frac{P(D, M \mid \vartheta)\, P_0(\vartheta \mid M)}{Z(D, M)}. \qquad (19)$$

In the above, $P(D, M \mid \vartheta)$ is known as the (experimental) likelihood, P_0 is the prior PDF of our parameters, and the evidence $Z(D, M)$ ensures the normalization of the posterior PDF. The label D refers to the dataset used in the fit (see Sect. 2.2) and the label M refers to the fit model (discussed below).

Our fit parameters can be classified as follows:

masses   We fix the bare mass of the $\psi(2S)$ to the physical world average $M_{\psi(2S)} = 3.6861$ GeV [10]. We fit the bare mass parameter of the $\psi(3770)$. This amounts to one fit parameter.

couplings   We fit the bare couplings of all resonances r listed in Eq. (15) to the channels listed in Eqs. (16) or (17), depending on the fit model. In the former setting the $\psi(2S)$ does not couple to the channel eff$_{\psi(3770)}$ and vice versa. In the latter both vector resonances couple to the same channel. In both cases this amounts to eight parameters describing the bare couplings.

background terms   We fit the background terms introduced in Eq. (9). In our analysis, only background terms for the processes $e^+e^- \to \{D^0\bar{D}^0, D^+D^-\}$ are considered. Symmetry of the K-matrix implies that we must use the same background terms for the time-reversed processes. This amounts to two independent fit parameters.

effective momentum   We fit the effective momentum q_0 entering Eq. (2). Although this quantity is a-priori channel dependent, we use a common value for q_0 across all channels. This amounts to one fit parameter.

By construction, all fit parameters are real-valued parameters as demanded by the properties of $\mathcal{K}$; see Sect. 2.1. We find that the likelihood (and hence the posterior PDF) exhibits several symmetries with respect to the above parameters that help in reducing the prior ranges of our analysis:

– If the effective channels are specific to a single resonance only and we do not impose a background term for them, the posterior PDF is insensitive to the signs of the effective couplings. In that case, we can choose both couplings to be positive. If, on the other hand, the effective channels are allowed to interfere, the relative sign between both couplings becomes observable. Hence, we choose the coupling to the $\psi(3770)$ to be positive.
– The posterior PDF is insensitive to the overall sign of the full set of bare couplings to a common resonance r, since each observable contains the product of two resonance couplings. Put differently, we can change the sign of all bare couplings g_k^r for a fixed r without changes to the posterior PDF. This enables us to choose the sign of one bare coupling per (fixed) resonance. We choose the couplings $g_{e^+e^-}^r$ to be positive.
– The posterior PDF is insensitive to the overall sign of the full set of couplings to a common single channel k. Put differently, we can change the sign of all bare couplings g_k^r for a fixed k without changes to the posterior PDF. This enables us to choose the sign of one bare coupling per (fixed) channel k. We choose the coupling $g_k^{\psi(3770)}$ to be positive.

We use as the prior PDF a product of uniform PDFs for each fit parameter.

We define the following fit models that are investigated as part of our analysis:

minimal   We fit the $\psi(3770)$ bare mass parameter and seven bare coupling parameters for the channels discussed above, fixing the coupling of the non-$D\bar{D}$ component of the $\psi(3770)$ (modelled by the eff$_{\psi(3770)}$ channel) to zero. (8 parameters)

nobackground   Same as the "minimal" model. We additionally fit the effective eff$_{\psi(3770)}$ channel. (9 parameters)

background   Same as the "no background" model. We additionally fit the constant background parameter in the off-diagonal K-matrix entries for the $e^+e^- \to D^0\bar{D}^0$ and $e^+e^- \to D^+D^-$ processes. Since our framework is constructed to produce a symmetric K-matrix, these background terms also contribute to the time-reversed processes $D^0\bar{D}^0 \to e^+e^-$ and $D^+D^- \to e^+e^-$. (11 parameters)

$q_0$variation   Same as the "background" model. We additionally fit the effective scale q_0, assuming, as stated above, that this parameter is the same for all the channels. (12 parameters)

interference   We fit the $\psi(3770)$ bare mass parameter and the eight bare coupling parameters as discussed above in the context of one joint effective channel with couplings to both the $\psi(2S)$ and the $\psi(3770)$, see Eq. (17). (11 parameters)

To carry out our analysis we use the EOS software [26] in version 1.0.11 [27], which has been modified for this purpose. Our analysis involves the optimisation of the posterior to determine the best-fit point or points. Since all experimental measurements used here are represented by a Gaussian likelihood, we compute the global χ^2 value in the best-fit point(s), providing a suitable test statistic for the fit.

We further produce importance samples of the model parameters for each fit model. This enables us to produce posterior-predictive distributions for dependent observables, including those used in the likelihood but also observables that are as-of-yet unmeasured. We produce the importance samples by application of the dynamical nested sampling algorithm [28]. To this end, EOS interfaces with the dynesty software [29,30]. Usage of dynamical nested sampling provides the additional benefit of estimating the evidence $Z(D, M)$ in parallel to sampling from the posterior density. This enables us to carry out a Bayesian model comparison between two models M_1 and M_2 for a common dataset D through computation of the Bayes factor

$$B(M_2, M_1) \equiv \frac{Z(D \mid M_2)}{Z(D \mid M_1)}. \tag{20}$$

A Bayes factor larger than unity favours model M_2 over model M_1. Jeffreys provides a more detailed interpretation of the Bayes factor [31].

Pole position To determine the position of the $\psi(3770)$ pole in the complex plane, we carry out a root finding procedure for $\det\left[1 - \mathcal{K}\,\Sigma^{\mathrm{II}}\right]$. To determine the uncertainty on the pole position, we repeat the procedure for each posterior sample.

Viability tests To test the accuracy of our numerical implementation, we perform three types of viability tests a-posteriori.

– Since our setup respects the unitarity of the S-matrix, we expect the sum of the partial decay widths to correspond to the total decay width, within the uncertainties of the fit.

– Since final state interaction is a long-distance effect, we expect the short-distance dominated residues of the resonance poles to factorize:

$$-\frac{1}{2\pi i} \oint_{C(s_r)} \mathcal{M}_{ab}^{\mathrm{II}}(s)\,ds = G_a^r \times G_b^r. \tag{21}$$

We remind that we extract the physical couplings G_k^r from their respective partial wave amplitudes $\mathcal{M}_{kk}^{\mathrm{II}}(s)$.

– The spectral function of the $\psi(3770)$ defined as [32, chapter 10.7]

$$\begin{aligned} \mathrm{spect}_{\psi(3770)}(s) = &-\frac{1}{\pi} \\ &\times \Im\left[\frac{1}{s - m_{\psi(3770)}^2 + \sum\left(g_k^{\psi(3770)}\right)^2 \Sigma_k(s)}\right], \end{aligned} \tag{22}$$

must be normalised, (i.e.) it must fulfill the property

$$\int_{s_{\mathrm{th}}}^{\infty} \mathrm{spect}_{\psi(3770)}(s)\,ds = 1, \tag{23}$$

where s_{th} is the first hadronic threshold.

Significant violation of either test would indicate potential issues with the numerical implementation of our framework. We apply these tests a-posteriori only, since the information needed to perform the test is not readily accessible in the course of the optimization of or the sampling from the posterior density. A numerical implementation may violate these tests due to loss of precision or use of functions outside their domain. This is meant as a practical test of the implementation, not a test of the physics.

Table 1 Summary of the analysis of each model. d.o.f. refers to the degrees of freedom, $\log(Z)$ to the Bayesian (natural-)log-evidence and $\mathcal{B}_{\text{non-}D\bar{D}}$ stands for $\mathcal{B}(\psi(3770) \to \text{non-}D\bar{D})$. In the last column, upper bounds are given at 90% probability

Model	χ^2	d.o.f.	p-value [%]	$\log(Z)$	$M_{\psi(3770)}$ [MeV]	$\Gamma_{\psi(3770)}$ [MeV]	$\mathcal{B}_{\text{non-}D\bar{D}}$ [%]
Minimal	120	119	46.0	82.0	3779.0 ± 0.3	23.5 ± 0.4	–
No background	120	118	44.0	79.0	3778.9 ± 0.3	23.6 ± 0.4	< 6.1
Background	107	116	71.8	81.7	3778.8 ± 0.3	25.0 ± 0.5	< 5.8
q_0 variation	106	115	71.8	69.3	3778.8 ± 0.3	24.6 ± 0.6	< 5.0
Interference	107	116	71.5	80.5	3778.8 ± 0.3	25.0 ± 0.5	< 6.1
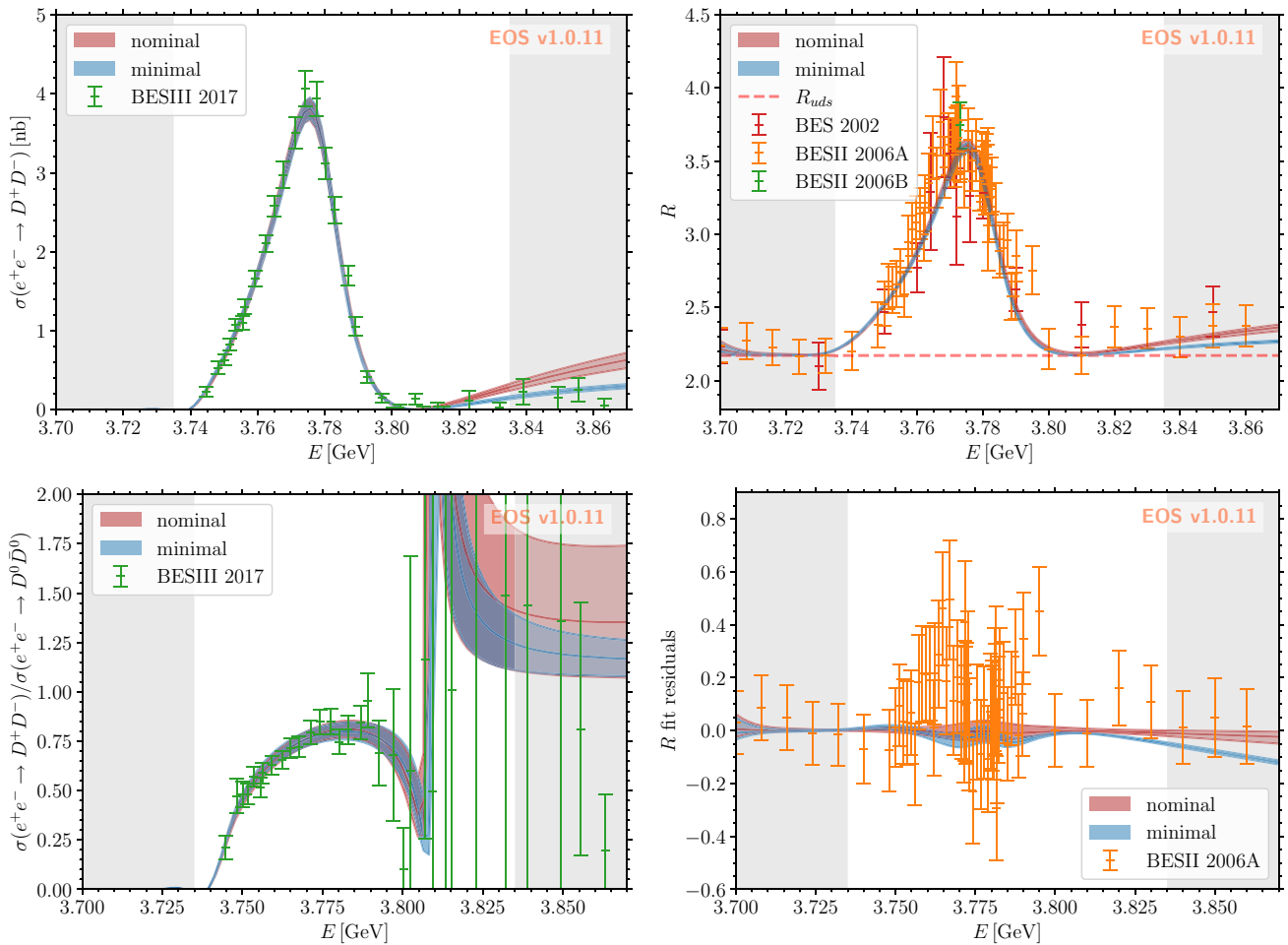
Fig. 1 Predictions of our minimal and nominal models (the "background" and "interference" models give indistinguishable shapes) for a couple of observables in the region of the $\psi(3770)$ resonance, compared to the experimental measurement performed by the BES experiment. Shaded areas are not used in the fit. Top left: Cross-section of the $e^+e^- \to D^+D^-$ scattering. *Top right: R-ratio. Bottom left:* Ratio of the cross-sections of $e^+e^- \to D^+D^-$ and $e^+e^- \to D^0\bar{D}^0$. The experimental points are given for illustrative purpose and neglect the experimental correlations between the D^+D^- and $D^0\bar{D}^0$ final states. Bottom right: Residuals of the fit of the R-ratio, the nominal "background" model is used for the subtraction and compared with the minimal model and experimental data

3 Results and interpretation

We perform a total of five analyses, using the dataset described in Sect. 2.2 and the five fit models described in Sect. 2.3. All five analyses yield satisfactory p-values larger than our a-priori threshold of 3%. The χ^2 and p-values are collected in Table 1, alongside the evidence $\log(Z)$ and our results for the $\psi(3770)$ mass and width. The best-fit points for all analyses pass the viability tests discussed in Sect. 2.3.

Our minimal fit model provides an excellent description of the data, with a *p*-value of 46% percent. To study model uncertainties for our fit parameters and derived quantities, we continue to investigate the remaining fit models. We first compare the three models that use two distinct effective channels, i.e., the models "no background", "background" and "q_0 variation". Although the "no background" model features the same χ^2 value as the "minimal" model, it is strongly disfavoured with respect to the latter according to Jeffreys' interpretation of the Bayes factor of $B(\text{no background, minimal}) \simeq 1/20$. The "background" model substantially improves the quality of the fit by decreasing χ^2 by 13 at the expense of 3 additional parameters. This leads to a preference in terms of the likelihood-ratio test by about 3σ while being as efficient in the description of the data as the "minimal" model with a Bayes factor of ~ 0.7. This is contrast to the "q_0 variation" model, which sees a similar improvement to the χ^2 value; however, it is disfavoured decisively by a Bayes factor of $3 \cdot 10^{-6}$ with respect to the "minimal" fit model. We therefore consider the results obtained in the "background" model as our nominal results in the case of two distinct effective channels.

The model "interference" with its description of the data with a single, interfering effective channel gives an equivalent fit quality compared to the "background" model but it is slightly less efficient in its description of the data: the Bayes factor yields

$$B(\text{background, interference}) \simeq 3.3,$$

which is "barely worth mentioning" according to Jeffreys' interpretation of the Bayes factor.

We thus see that the "background" and the "interference" models both provide an excellent description of the data although the former is somewhat favoured. The distinction of the two is that in the "background" model the two vector resonances included in the model cannot interfere via the non-$D\bar{D}$ channels while in the "interference" model they can. In this sense, the two models provide two extreme scenarios: one assumes that the decay channels of the resonances are all distinct, the other that they are identical. We therefore expect the spread of our results in either model to cover the true physical results. A further investigation of this issue would mandate a fit to the respective set of physical exclusive non-$D\bar{D}$ modes.

The posterior samples for both models are available in form of machine-readable files upon request. No sizable departure from Gaussian distributions are found in the posterior and all samples pass the viability tests discussed in Sect. 2.3.

We present the predictions of both models in Fig. 1. In the upper plots, the cross-section of $e^+e^- \to D^+D^-$ scattering and the *R*-ratio are compared to the experimental data used in the fit. The shaded regions indicate the data not used in the

fit. In the bottom right plot, we show the fit residuals for the *R*-ratio. It is obtained by subtracting the *R*-ratio line shape of our nominal best fit from both the experimental data and the predictions in the "background" and "interference". The residual excess of the data around $E = 3.765$ GeV motivated the interpretation of the $\psi(3770)$ as a double pole [33]. Our results show that the data can be fully explained by interference effects between the $\psi(3770)$ with the $\psi(2S)$ resonance, an effect not included in Ref. [33].[1]

Our results deviate from those of Ref. [12] in various aspects: while in our case the parameter in the regulator functions does not play a significant role as is expected, since the line shape should be dominated by the resonance itself, in that work it was determined with a 1% accuracy. This means that in Ref. [12] the regulator plays a crucial role to shape the resonance. Our fits only need the well established $\psi(2S)$ and $\psi(3770)$ as poles of the amplitude, while the fits of Ref. [12], where the $\psi(2S)$ was omitted, dynamically generate an additional pole. The authors stress that this emergence is unavoidable, if one wants to get a good description of the data. However, our analysis shows that high-accuracy descriptions of the data are possible even in scenarios without that additional pole, as long as the $\psi(2S)$ is included in the analysis. Thus, we may conclude that the interplay of an additional pole with that of the $\psi(3770)$ is indeed necessary to understand the line shape of the latter, however, this additional pole can well be an established charmonium state.

Mass and width Within both of our nominal fit models, we obtain for the physical mass and total decay width of the $\psi(3770)$ identical results:

$$
\begin{aligned}
M_{\psi(3770)} &= 3778.8 \pm 0.3 \,\text{MeV} \\
\Gamma_{\psi(3770)} &= 25.0 \pm 0.5 \,\text{MeV}.
\end{aligned}
\tag{24}
$$

These values are consistent with those extracted in Ref. [12]

$$
\begin{aligned}
M^{12}_{\psi(3770)} &= 3777.0 \pm 1.0 \,\text{MeV} \\
\Gamma^{12}_{\psi(3770)} &= 24.6 \pm 1.0 \,\text{MeV}.
\end{aligned}
\tag{25}
$$

The stability of the pole location is very reassuring, given that there are significant differences in the actual modelling of the non-$\psi(3770)$ physics between our work and Ref. [12], as outlined above.

We remind that our results are obtained from a *K*-matrix analysis. They are therefore not expected to reflect the parameters extracted from Breit–Wigner analyses, such as the one of Ref. [9] or the world average quoted in the PDG review [10]. Nevertheless, we provide these respective results here for convenience

$$
\begin{aligned}
M^{9}_{\psi(3770)} &= 3779.8 \pm 0.6 \,\text{MeV} \\
\Gamma^{9}_{\psi(3770)} &= 25.8 \pm 1.3 \,\text{MeV},
\end{aligned}
\tag{26}
$$

---

[1] It is not clear to us if the analysis presented in Ref. [33] uses further experimental data that is not publicly available.
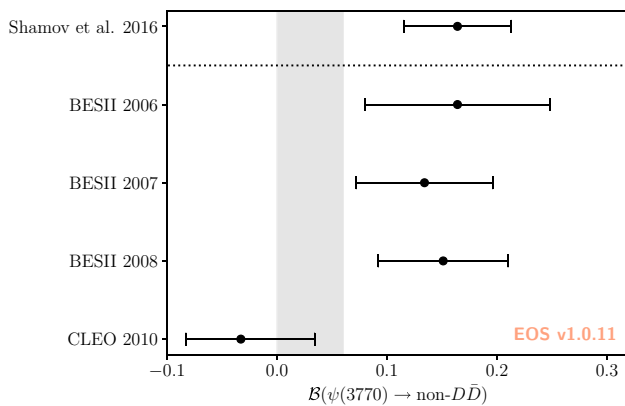
Fig. 2 Comparison of our upper bound on the branching ratio of the $\psi(3770)$ to non-$D\bar{D}$ final states at 90% probability (grey band) with results from the phenomenological literature [9] above the dotted line and the experimental literature [34–37] below. Although they use different analysis techniques, the three results by the BESII experiment are not statistically independent

and

$$
\begin{aligned}
M_{\psi(3770)}^{10} &= 3778.1 \pm 0.7\,\text{MeV} \\
\Gamma_{\psi(3770)}^{10} &= 27.5 \pm 0.9\,\text{MeV}.
\end{aligned}
\tag{27}
$$

We find both the mass and the total decay width to be quite compatible with the literature. Given the variety of theoretical approaches to describe the data, we do not consider it meaningful to quote a statistical significance for the deviations.

Branching ratio of the $\psi(3770)$ to non-$D\bar{D}$ As already discussed in the literature [9,34–37], the combined analysis of inclusive and exclusive measurements allows for a non-vanishing coupling of the $\psi(3770)$ to non-$D\bar{D}$ channels, i.e., yielding $\mathcal{B}(\psi(3770) \to \text{non-}D\bar{D})$ at the level of a few percent. Our results for this branching ratio are presented in the last row of Table 1. Finding good agreement between the upper bounds in our two nominal fit models, we summarize our finding as

$$
\mathcal{B}(\psi(3770) \to \text{non-}D\bar{D}) < 6\% \text{ at } 90\% \text{ probability}.
\tag{28}
$$

We juxtapose this results with those quoted in the literature in Fig. 2. We find that our result is systematically lower than what is found in the literature, with the exception of the results of Ref. [37]. We mention in passing that using the exclusive observed cross section instead of the exclusive Born cross section leads to an artificially enhanced non-$D\bar{D}$ contribution of the level of $\sim 20\%$.

Isospin symmetry at the $\psi(3770)$ pole The $\psi(3770)$ resonance lies just above the $D^0\bar{D}^0$ threshold ($\sqrt{s} \sim 3.73\,\text{GeV}$) and the D^+D^- threshold ($\sqrt{s} \sim 3.74\,\text{GeV}$). It is therefore sensitive to the differences in phase space volume between the two channels, leading to an apparent violation of isospin symmetry in the ratio of the exclusive cross sections; see the

bottom left plot of Fig. 1 for an illustration. We prefer to probe the degree of isospin symmetry violation at hand of a quantity that is unaffected by these phase space effects. To this end, we investigate the ratio of the bare couplings between this resonance and either of the two channels. Unbroken isospin symmetry would yield unity, with symmetry breaking corrections being naturally suppressed by powers of α_e and $(m_u - m_d)/m_s$.

We find the ratio of bare couplings to be

$$
g_{D^0\bar{D}^0}^{\psi(3770)}/g_{D^+D^-}^{\psi(3770)} = 0.99 \pm 0.03,
\tag{29}
$$

showing no sign of isospin symmetry violation in these decays in either model. We therefore conclude that the structure shown in the bottom plot of Fig. 1 originates from the difference in the phase space volumes. Our finding is in tension with findings in the literature [23,38], which are obtained by fitting a Breit–Wigner-like line shape to the $\psi(3770)$ spectrum, but in line with the findings of Ref. [12]. In addition, we determine the isospin ratio of the bare $D\bar{D}$ couplings to the $\psi(2S)$ resonance to be 1.02 ± 0.10, which is also compatible with unity with substantially larger uncertainties. The larger uncertainty obtained in this ratio is likely due to the fact that we are not fully modelling the $\psi(2S)$ resonance, as described in Sect. 2.1.

4 Summary and outlook

In this paper we have performed a coupled-channel analysis of $e^+e^- \to$ open charm processes in a window around the $\psi(3770)$. Our analysis compares different models based on the K-matrix framework. We find that the now available high-resolution measurements by the BES, BESII, and BESIII experiments can be described very well within our models. We have found no indication for a sizable branching ratio to non-$D\bar{D}$ final states. Modelling these non-$D\bar{D}$ channels with a single effective P-wave channel, we set an upper bound

$$
\mathcal{B}(\psi(3770) \to \text{non-}D\bar{D}) < 6\% \text{ at } 90\% \text{ probability}.
$$

Our result is compatible with but systematically smaller than nearly all other determinations of this branching fraction. In recent years, various vector states were identified as good candidates for exotic states beyond the quark model—see Refs. [2–7] for recent reviews. However, given our results we see no reason to question a dominant $\bar{c}c$ nature of the $\psi(3770)$. Note that hadronic loops that drive e.g. the emergence of hadronic molecules [5] are suppressed near threshold since they appear in a P-wave.

In the course of our analysis, we have struggled at times with the lack of statistical constraints on the electron couplings $g_{e^+e^-}^r$. For this coupling to the $\psi(2S)$ we had to resort to external determinations of the partial width $\Gamma(\psi(2S) \to$

e^+e^-). We would like to point out that this caveat could be overcome by using measurements of the cross section $e^+e^- \to \mu^+\mu^-$ in our phase space of interest, which are currently not available at the level of precision we require.

We look forward to future work in this field, where we plan to extend our analysis to larger values of $\sqrt{s}$ and, accordingly, to both additional channels and resonances. This extension will be essential for an envisaged phenomenological application: the transfer of the line shape information for the vector charmonia from measurements of $e^+e^- \to$ hadrons cross sections to theoretical predictions of exclusive $b \to s\ell^+\ell^-$ decays. A sketch of this application is provided in the appendix of this work. It is presently unclear if this application can be achieved without non-public information on the experimental measurements, and we hope that this work reinvigorates interest amongst our experimental colleagues.

A Relations to non-local form factors in $b \to s\ell^+\ell^-$

Non-local hadronic matrix elements in exclusive $b \to s\ell^+\ell^-$ processes pose a major source of systematic uncertainty to their theoretical predictions [39]. They have been the focus of

theoretical developments for the past decade [40–46]. Using $\bar{B} \to \bar{K}\ell^+\ell^-$ processes as an example for definiteness, a common definition of the dominant (charm-induced) non-local[2] contributions reads

$$\mathcal{H}^\mu = i \int d^4x \, e^{iq\cdot x}$$
$$\langle \bar{K}(k)| \, T\{\bar{c}\gamma^\mu c(x), \sum_i C_i O_i(0)\} |\bar{B}(q+k)\rangle \,. \quad \text{(A.1)}$$

Here the O_i are a set of local operators in the weak effective theory of mass dimension six and with flavour quantum numbers $sbcc$,

$$O_i = [\bar{s}\Gamma_i b][\bar{c}\tilde{\Gamma}_i c], \quad \text{(A.2)}$$

with combined Dirac and colour structures Γ_i and $\tilde{\Gamma}_i$; the C_i are their respective Wilson coefficients. It is convenient to discuss this hadronic matrix element in terms of its scalar-valued non-local form factors

$$\mathcal{H}_{(\lambda)}(q^2) = P^\mu(\lambda)\,\mathcal{H}_\mu(q). \quad \text{(A.3)}$$

Here $\lambda = 0, \pm 1$ denotes a polarization state of the virtual photon coupling to the vector current, and $P^\mu(\lambda)$ are suitable projection operators; we refer to Ref. [46] for their definition. We emphasize that the $\mathcal{H}_{(\lambda)}$ are complex-valued functions even below all thresholds in q^2. This property emerges since the $\bar{B}$ meson can decay into an on-shell hadronic state by virtue of the four-quark operators O_i; see Ref. [40] for a discussion on this topic.

A systematic approach to describing $\mathcal{H}_{(\lambda)}(q^2)$ for $q^2 < 4M_D^2$ has been developed over the course of the last decade [44–46]. Here, we instead focus on the open-charm region $q^2 \geq 4M_D^2$. Common approaches to estimate or describe the non-local form factors in this region include an operator product expansion (OPE) of the time-ordered product in Eq. (A.1) [47,48], and a Breit–Wigner model of the broad charmonium resonance therein [49–51]. We propose a different approach based on the P-vector formalism that utilizes the information obtained in the main part of this work. First, we note that by crossing symmetry the scalar non-local form factors can be related to the scattering amplitude $\bar{B}K \to e^+e^-$

$$\mathcal{A}_{\bar{B}K, e^+e^-} \sim \sum_\lambda L_\mu P^{*\mu}_{(\lambda)} \mathcal{H}_\lambda, \quad \text{(A.4)}$$

where $L_\mu = \bar{u}_\ell \gamma_\mu v_\ell$ denotes the leptonic current. Similarly, the P-wave amplitude for the processes $\bar{B} \to \bar{K}D\bar{D}$ can be related to $\bar{B}K \to D\bar{D}$ scattering amplitudes $\mathcal{A}_{\bar{B}K, D\bar{D}}$. Both of these processes are induced only by the weak interaction. As a consequence, their contributions to the overall width

---

2   Here and in the jargon of the rare $b \to s\ell^+\ell^-$ decays, "non-local" refers to the fact that the operator in Eq. (A.1) has a non-trivial x dependence, opposed to the local $\bar{s} \ldots b$ operators whose matrix elements dominate the description of theses processes off-resonance.

of the various vector charmonium resonances in the unitarization, for example through the K-matrix approach, are negligible. In such cases, the P-vector formalism provides a convenient approach to parametrize both of the amplitudes mentioned above:

$$\mathcal{A}_{\bar{B}K,a} = n_a \left[1 - \mathcal{K}\Sigma\right]^{-1} P_{\bar{B}K}(s). \tag{A.5}$$

In the above $P_{\bar{B}K}$ represents the source term,

$$P_{\bar{B}K}(s) = \sum_r^{N_R} \frac{\alpha^r g_{\bar{B}K}^r}{m_r^2 - s} + b_{\bar{B}K} \tag{A.6}$$

split into a sum of the same resonances accounted for by the K-matrix and a background term $b_{\bar{B}K}$. As before, m_r and g_r represent bare masses and couplings, and the mass parameters should match those used in the K-matrix analysis. In contrast to the usual P-vector formalism, the couplings $g_{\bar{B}K}^r$ and the background term $b_{\bar{B}K}$ are complex-valued quantities. This can be readily understood from the fact that non-local form factors (and hence the scattering amplitudes) feature non-vanishing imaginary parts below all thresholds, as discussed above.

References

1. O. Bar, U.J. Wiese, Can one see the number of colors? Nucl. Phys. B **609**, 225 (2001). https://doi.org/10.1016/S0550-3213(01)00288-7. arxiv:hep-ph/0105258
2. R.F. Lebed, R.E. Mitchell, E.S. Swanson, Heavy-quark QCD exotica. Prog. Part. Nucl. Phys. **93**, 143 (2017). https://doi.org/10.1016/j.ppnp.2016.11.003. arxiv:1610.04528
3. A. Esposito, A. Pilloni, A.D. Polosa, Multiquark resonances. Phys. Rep. **668**, 1 (2017). https://doi.org/10.1016/j.physrep.2016.11.002. arxiv:1611.07920
4. S.L. Olsen, T. Skwarnicki, D. Zieminska, Nonstandard heavy mesons and baryons: experimental evidence. Rev. Mod. Phys. **90**, 015003 (2018). https://doi.org/10.1103/RevModPhys.90.015003. arxiv:1708.04012
5. F.-K. Guo, C. Hanhart, U.-G. Meißner, Q. Wang, Q. Zhao, B.-S. Zou, Hadronic molecules. Rev. Mod. Phys. **90**, 015004 (2018). https://doi.org/10.1103/RevModPhys.90.015004. arxiv:1705.00141
6. N. Brambilla, S. Eidelman, C. Hanhart, A. Nefediev, C.-P. Shen, C.E. Thomas et al., The XYZ states: experimental and theoretical status and perspectives. Phys. Rep. **873**, 1 (2020). https://doi.org/10.1016/j.physrep.2020.05.001. arxiv:1907.07583
7. H.-X. Chen, W. Chen, X. Liu, Y.-R. Liu, S.-L. Zhu, An updated review of the new hadron states. Rep. Prog. Phys. **86**, 026201 (2023). https://doi.org/10.1088/1361-6633/aca3b6. arxiv:2204.02649
8. T. Aoyama et al., The anomalous magnetic moment of the muon in the Standard Model. Phys. Rep. **887**, 1 (2020). https://doi.org/10.1016/j.physrep.2020.07.006. arxiv:2006.04822
9. A.G. Shamov, K.Y. Todyshev, Analysis of BaBar, Belle, BES-II, CLEO and KEDR data on $\psi(3770)$ line shape and determination of the resonance parameters. Phys. Lett. B **769**, 187 (2017). https://doi.org/10.1016/j.physletb.2017.03.057. arxiv:1610.02147
10. Particle Data Group Collaboration, Rev. Part. Phys. PTEP **2022**, 083C01 (2022). https://doi.org/10.1093/ptep/ptac097
11. T.V. Uglov, Y.S. Kalashnikova, A.V. Nefediev, G.V. Pakhlova, P.N. Pakhlov, Exclusive open-charm near-threshold cross sections in a coupled-channel approach. JETP Lett. **105**, 1 (2017). https://doi.org/10.1134/S0021364017010064. arxiv:1611.07582
12. S. Coito, F. Giacosa, Line-shape and poles of the $\psi(3770)$. Nucl. Phys. A **981**, 38 (2019). https://doi.org/10.1016/j.nuclphysa.2018.10.083. arxiv:1712.00969
13. S.U. Chung, J. Brose, R. Hackmann, E. Klempt, S. Spanier, C. Strassburger, Partial wave analysis in K matrix formalism. Annalen Phys. **4**, 404 (1995). https://doi.org/10.1002/andp.19955070504
14. N.N. Achasov, G.N. Shestakov, Electronic width of the $\psi(3770)$ resonance interfering with the background. Phys. Rev. D **103**, 076017 (2021). https://doi.org/10.1103/PhysRevD.103.076017. arxiv:2102.03738
15. J.M. Blatt, V.F. Weisskopf, *Theoretical Nuclear Physics* (Springer, New York, 1952). https://doi.org/10.1007/978-1-4612-9959-2
16. BaBar Collaboration, Study of the exclusive initial-state-radiation production of the $D\bar{D}$ system. arxiv:0710.1371
17. Belle Collaboration, Measurement of the near-threshold $e^+e^- \to D\bar{D}$ cross section using initial-state radiation. Phys. Rev. D **77**, 011103 (2008). https://doi.org/10.1103/PhysRevD.77.011103. arxiv:0708.0082
18. BES Collaboration, Measurements of the cross-section for $e^+e^- \to$ hadrons at center-of-mass energies from 2 GeV to 5 GeV. Phys. Rev. Lett. **88**, 101802 (2002). https://doi.org/10.1103/PhysRevLett.88.101802. arxiv:hep-ex/0102003
19. M. Ablikim et al., Measurements of the continuum R(UDS) and R values in e^+e^- annihilation in the energy region between 3.650 and 3.872 GeV,. Phys. Rev. Lett. **97**, 262001 (2006). https://doi.org/10.1103/PhysRevLett.97.262001. arxiv:hep-ex/0612054
20. BESIII Collaboration, Measurement of the Cross Section for $e^+e^- \to$ Hadrons at Energies from 2.2324 to 3.6710 GeV. Phys. Rev. Lett. 128 062004 (2022). https://doi.org/10.1103/PhysRevLett.128.062004. arxiv:2112.11728
21. CLEO Collaboration, Measurement of charm production cross sections in e^+e^- annihilation at energies between 3.97 and 4.26 GeV. Phys. Rev. D **80**, 072001 (2009). https://doi.org/10.1103/PhysRevD.80.072001. arxiv:0801.3418
22. BES Collaboration, Measurements of the cross-sections for $e^+e^- \to$ hadrons at 3.650 GeV, 3.6648 GeV, 3.773 GeV and the branching fraction for $\psi(3770) \to$ non-$D\bar{D}$. Phys. Lett. B **641**, 145 (2006). https://doi.org/10.1016/j.physletb.2006.08.049. arxiv:hep-ex/0605105
23. A.J. Julin, Measurement of $D\bar{D}$ decays from the $\psi(3770)$ resonance. Ph.D. thesis, Minnesota U. (2017). https://hdl.handle.net/11299/199064
24. N. Hüsken, R.F. Lebed, R.E. Mitchell, E.S. Swanson, Y. Wang, C.-Z. Yuan, Work in preparation
25. R.V. Harlander, M. Steinhauser, rhad: a program for the evaluation of the hadronic R ratio in the perturbative regime of QCD. Comput. Phys. Commun. **153**, 244 (2003). https://doi.org/10.1016/S0010-4655(03)00204-2. arxiv:hep-ph/0212294
26. EOS AUTHORS Collaboration, EOS: a software for flavor physics phenomenology. Eur. Phys. J. C **82**, 569 (2022). https://doi.org/10.1140/epjc/s10052-022-10177-4. arxiv:2111.15428
27. D. van Dyk, M. Reboud, N. Gubernari, P. Lüghausen, D. Leljak, A. Kokulu et al., EOS version 1.0.11 (Zenodo, 2024). https://doi.org/10.5281/zenodo.10600399
28. E. Higson, W. Handley, M. Hobson, A. Lasenby, Dynamic nested sampling: an improved algorithm for parameter estimation and evidence calculation. Stat Comput **29**, 891 (2018). https://doi.org/10.1007/s11222-018-9844-0
29. J.S. Speagle, dynesty: a dynamic nested sampling package for estimating Bayesian posteriors and evidences. Mon. Not. Roy. Astron. Soc. **493**, 3132 (2020). https://doi.org/10.1093/mnras/staa278

30. S. Koposov, J. Speagle, K. Barbary, G. Ashton, E. Bennett, J. Buchner et al., dynesty version 2.0.3, Dec. (2022). https://doi.org/10.5281/zenodo.7388523

31. H. Jeffreys, *The Theory of Probability, Oxford Classic Texts in the Physical Sciences* (Oxford University Press, Oxford, 1939)

32. S. Weinberg, *The Quantum Theory of Fields. Vol. 1: Foundations* (Cambridge University Press, Cambridge, 2005). https://doi.org/10.1017/CBO9781139644167

33. M. Ablikim et al., Anomalous line shape of the cross section for $e^+e^- \to$ hadrons in the center-of-mass energy region between 3.650 and 3.872 GeV,. Phys. Rev. Lett. **101**, 102004 (2008). https://doi.org/10.1103/PhysRevLett.101.102004

34. BES Collaboration, Direct measurements of the cross sections for $e^+e^- \to$ hadrons(non-$D\bar{D}$) in the range from 3.65 GeV to 3.87 GeV and the branching fraction for $\psi(3770) \to$ non-$D\bar{D}$. Phys. Lett. B **659**, 74 (2008). https://doi.org/10.1016/j.physletb.2007.11.078

35. M. Ablikim et al., Direct measurements of the non-$D\bar{D}$ cross section $\sigma_{\psi(3770) \to \text{non-}D\bar{D}}$ at $E_{cm} = 3.773$ GeV and the branching fraction for $\psi(3770) \to$ non-$D\bar{D}$. Phys. Rev. D **76**, 122002 (2007). https://doi.org/10.1103/PhysRevD.76.122002

36. BES Collaboration, Measurements of the branching fractions for $\psi(3770) \to D^0\bar{D}^0, D^+D^-, D\bar{D}$ and the resonance parameters of $\psi(3770)$ and $\psi(2S)$. Phys. Rev. Lett. **97**, 121801 (2006). https://doi.org/10.1103/PhysRevLett.97.121801. arxiv:hep-ex/0605107

37. CLEO Collaboration, Measurement of $\sigma(e^+e^- \to \psi(3770) \to$ hadrons) at $E_{c.m.} = 3773$ MeV. Phys. Rev. Lett. **96**, 092002 (2006). https://doi.org/10.1103/PhysRevLett.96.092002. arxiv:1004.1358

38. K. Ishikawa, O. Jinnouchi, K. Nishiwaki, K.-Y. Oda, Wave-packet effects: a solution for isospin anomalies in vector-meson decay. Eur. Phys. J. C **83**, 978 (2023). https://doi.org/10.1140/epjc/s10052-023-12077-7. arxiv:2308.09933

39. F. Gross et al., 50 years of quantum chromodynamics. arxiv:2212.11107

40. A. Khodjamirian, T. Mannel, A.A. Pivovarov, Y.M. Wang, Charm-loop effect in $B \to K^{(*)}\ell^+\ell^-$ and $B \to K^*\gamma$. JHEP **09**, 089 (2010). https://doi.org/10.1007/JHEP09(2010)089. arxiv:1006.4945

41. A. Khodjamirian, T. Mannel, Y.M. Wang, $B \to K\ell^+\ell^-$ decay at large hadronic recoil. JHEP **02**, 010 (2013). https://doi.org/10.1007/JHEP02(2013)010. arxiv:1211.0234

42. S. Jäger, J. Martin Camalich, On $B \to V\ell\ell$ at small dilepton invariant mass, power corrections, and new physics. JHEP **05**, 043 (2013). https://doi.org/10.1007/JHEP05(2013)043. arxiv:1212.2263

43. M. Ciuchini, M. Fedele, E. Franco, S. Mishima, A. Paul, L. Silvestrini et al., $B \to K^*\ell^+\ell^-$ decays at large recoil in the Standard Model: a theoretical reappraisal. JHEP **06**, 116 (2016). https://doi.org/10.1007/JHEP06(2016)116. arxiv:1512.07157

44. C. Bobeth, M. Chrzaszcz, D. van Dyk, J. Virto, Long-distance effects in $B \to K^*\ell\ell$ from analyticity. Eur. Phys. J. C **78**, 451 (2018). https://doi.org/10.1140/epjc/s10052-018-5918-6. arxiv:1707.07305

45. N. Gubernari, D. van Dyk, J. Virto, Non-local matrix elements in $B_{(s)} \to \{K^{(*)}, \phi\}\ell^+\ell^-$. JHEP **02**, 088 (2021). https://doi.org/10.1007/JHEP02(2021)088. arxiv:2011.09813

46. N. Gubernari, M. Reboud, D. van Dyk, J. Virto, Improved theory predictions and global analysis of exclusive $b \to s\mu^+\mu^-$ processes. JHEP **09**, 133 (2022). https://doi.org/10.1007/JHEP09(2022)133. arxiv:2206.03797

47. B. Grinstein, D. Pirjol, Exclusive rare $B \to K^*\ell^+\ell^-$ decays at low recoil: controlling the long-distance effects. Phys. Rev. D **70**, 114005 (2004). https://doi.org/10.1103/PhysRevD.70.114005. arxiv:hep-ph/0404250

48. M. Beylich, G. Buchalla, T. Feldmann, Theory of $B \to K^{(*)}\ell^+\ell^-$ decays at high q^2: OPE and quark-hadron duality. Eur. Phys. J. C **71**, 1635 (2011). https://doi.org/10.1140/epjc/s10052-011-1635-0. arxiv:1101.5118

49. F. Kruger, L.M. Sehgal, Lepton polarization in the decays $B \to X(s)\mu^+\mu^-$ and $B \to X(s)\tau^+\tau^-$. Phys. Lett. B **380**, 199 (1996). https://doi.org/10.1016/0370-2693(96)00413-3. arxiv:hep-ph/9603237

50. J. Lyon, R. Zwicky, Resonances gone topsy turvy—the charm of QCD or new physics in $b \to s\ell^+\ell^-$?. arXiv:1406.0566

51. S. Braß, G. Hiller, I. Nisandzic, Zooming in on $B \to K^*\ell\ell$ decays at low recoil. Eur. Phys. J. C **77**, 16 (2017). https://doi.org/10.1140/epjc/s10052-016-4576-9. arxiv:1606.00775